Biomaterials Science

Accepted Manuscript

This article can be cited before page numbers have been issued, to do this please use: Y. Opoku-Damoah, R. Zhang, H. T. Ta and Z. P. Xu, *Biomater. Sci.*, 2021, DOI: 10.1039/D1BM00941A.

ROYAL SOCIETY OF CHEMISTRY

rsc.li/biomaterials-science

Vitamin E-facilitated Carbon Monoxide Pro-drug Nanomedicine for Efficient Light-Responsive Combination Cancer Therapy

View Article Online
DOI: 10.1039/D1BM00941A

Yaw Opoku-Damoah [1], Run Zhang [1,], Hang T. Ta [1,2,3], and Zhi Ping Xu[1, *]*

[1] Australian Institute for Bioengineering and Nanotechnology, The University of Queensland, Brisbane, QLD 4072, Australia.

[2] School of Environment and Science, Griffith University, Brisbane, QLD 4111, Australia

[3] Queensland Micro and Nanotechnology Centre, Griffith University, Brisbane, QLD 4111, Australia

Corresponding authors:

Tel: +61 7 334 63809; E-mail: gordonxu@uq.edu.au; r.zhang@uq.edu.au.

Abstract

View Article Online
DOI: 10.1039/D1BM00941A

The quest to maximize therapeutic efficiency in cancer treatment requires innovative delivery nanoplatforms capable of employing different modules simultaneously. Combination therapy has proven to be one of the best anticancer strategies so far. Herein, we have developed a lipid-encapsulated nanoplatform that combines chemotherapy with photoresponsive gas therapy for colon cancer treatment. Carbon monoxide releasing molecule (CORM) and vitamin E analogues (pure/pegylated α-tocopheryl succinate; α-TOS) were co-loaded into the lipid layer with core-shell upconversion nanoparticles (UCNPs), which converted 808 nm lights to 360 nm photons to trigger CO release at the tumor site. This folic acid (FA)-targeting nanomedicine (Lipid/UCNP/CORM/α-TOS/FA: LUCTF) possessed cancer-targeting ability and light-triggered CO release ability for synergistic apoptosis of HCT116 cells *via* enhanced ROS generation and mitochondria membrane breaking. *In vivo* data have confirmed the significantly enhanced therapeutic efficacy of LUCTF without any significant biosafety issues after intravenous administration. Thus, nanomedicine LUCTF represents a novel way for efficient cancer therapy via combining locally released CO and a compatible chemotherapeutic agent (e.g. α-TOS).

Keywords: combination therapy, gas therapy, vitamin E analogues, chemotherapy, carbon monoxide releasing molecule, upconversion nanoparticle.

View Article Online
DOI: 10.1039/D1BM00941A

1 Introduction

The complexity of cancer is gradually leading to the advent of innovative nano-inspired combination therapies to circumvent the malignant pathways and associated multidrug resistance (MDR) [1, 2]. Recent research has suggested that a combination of biocompatible drugs in one delivery system is gradually becoming one of the best ways to combat cancer [3]. If two cancer drugs are functionally complementary and the therapeutic outcomes contributed by each individual drug at a specified dose are statistically independent, then a better therapeutic outcome for the combination would be produced [4]. More importantly, with the recent advances in targeted nano-based delivery systems, co-loading multiple cancer drugs in one nano-delivery system has been pursued for better treatment outcomes [5, 6]. Maximizing the therapeutic effect of a delivery nano-system should also take into consideration the biocompatibility, synergy and ease of fabrication to produce a suitable nanoformulation for cost-effective combination cancer therapy.

Gas therapy has gained much attention in recent years, despite not being extensively explored due to the difficulty in handling and delivering such gaseous agents to the required targeted site [7, 8]. With the convincing data suggesting that gases such as carbon monoxide (CO) have significant therapeutic potentials in various diseases, carbon monoxide releasing molecules (CORM) were developed with various stimuli to trigger CO release at required sites for cancer therapy [9, 10]. CO's therapeutic potentials include its ability to target the mitochondria in tumor cells by consuming the limited amount of oxygen and triggering the generation of reactive oxygen species (ROS) to cause mitochondrial collapse [11, 12]. Its involvement in the down-regulation of pro-inflammatory proteins such as interleukin 1β/tumor necrosis factor-α was also documented previously. [13]. CO produces an anti-Warburg effect by rapidly aiding tumor bioenergetics, which usually ends up in metabolic exhaustion. However, the difficulty in handling and releasing CO molecules remains the

greatest challenge. Many researchers have attempted to overcome this challenge by preparing CORMs for stimuli-triggered CO release *via* enzyme action, pH-sensitivity, photoresponsiveness or solvent solvation [14]. It is becoming increasingly evident that photo-responsive CO systems (photoCORMs) are better positioned to be readily translated into CO therapeutic candidates due to the light responsiveness, biosafety and efficiency in releasing CO molecules at the required local site. As CO release is often triggered by direct UV lights [15-17], the penetration depth and the associated skin damage are of great concern. Thus, if near-infrared (NIR) light can act similarly to the UV light (360 nm) in this responsive nanosystem, the skin damage will be minimized and the penetration will be deeper [18]. We have previously demonstrated that upconversion nanoparticles (UCNPs) can be engineered to absorb NIR lights and upconvert to photons in the UV region to trigger CO release from CORMs [19], which is more efficient than many other systems [20, 21]. Moreover, engineering 980 nm-absorbing UCNPs to absorb 808 nm laser prevents water absorption and overheating in tissues [22, 23]. However, an enhancement for optimal cancer therapy *in vivo* is prudent for future clinical translation.

On the other hand, chemotherapeutic agents have proven to be compatible with most photoresponsive agents to satisfy the requirement for synergy. For instance, hydrophobic vitamin E analogues such as α-tocopheryl succinate (α-TOS) and its soluble pegylated form (TPGS) have been explored for their incorporation into biofriendly lipid systems for cancer therapy. α-TOS is capable of inhibiting cell proliferation and induces cellular apoptosis [24, 25], probably by aiding reactive oxygen species (ROS) generation [26-28]. α-TOS may also cause the mitochondrial membrane permeable and subsequently produce cytochrome c [29-31]. Vitamin E analogues can easily form part of the hydrophilic layer of lipid formulations [32, 33], and synergize with DOX [34]. Wu et al. also demonstrated that α-TOS was

View Article Online
DOI: 10.1039/D1BM00941A

easily integrated in a lipid delivery system with 15 wt% as the most optimal formulation with IFN-γ [35].

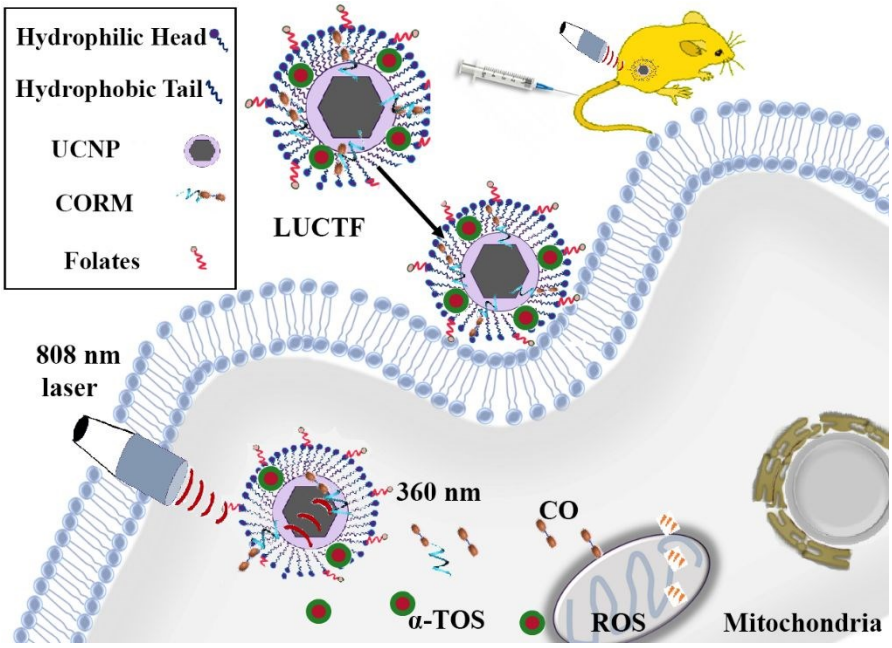

Scheme 1. Schematic diagram of CO release molecules (CORMs) encapsulated in lipid bilayers with upconversion nanoparticles playing a mediatory role to absorb photons from 808 nm lights to produce UV photons capable of triggering CO release from CORMs. Folic acids (FA) in the lipid nanoformulation target cancer cells with overexpressed FA receptor.

Herein, this study seeks to develop a robust delivery system to co-load two therapeutic agents (CORM-$C_{30}H_{49}N_3Mn(CO)_3$ Br and α-TOS) for combination cancer therapy. α-TOS was selected to complement CORM for NIR-mediated combined gas chemotherapy, with the capacity to support the co-encapsulation in a lipid delivery system for an enhanced therapeutic effect [36]. The aim is to synergistically induce apoptosis by attacking the mitochondria of cancer cells through different mechanisms [37, 38]. Their combined effect is expected to increase the ROS generation for cancer cell death. As shown in **Scheme 1**, the lipid-based nanoplatform (Lipid/UCNP/CORM/α-TOS /FA: LUCTF) can target HCT-116 cancer cells *via* folic acid (FA)-FA receptor interactions and released CO (mediated by 808

nm light irradiation) to induce cancer cell death by synergistic actions of α-TOS. Both *in vitro* and *in vivo* data demonstrated the high therapeutic potential and safety of this nanoformulation under irradiation of 808 nm laser at 1.0 W/cm^2 for 5 min.

2 Experimental Section

2.1 Synthesis of lipid nanoformulation

Core-shell UCNP was prepared by the thermal decomposition method described previously [19]. CORM was also prepared according to the procedure in Sakla et al. [39]. Thin film hydration method was employed to formulate LUCTF lipid nanoparticles, as detailed in Table 1. Briefly, 1.5 mg of lipid mixture (DOPC, DOPA, Cholesterol, DSPE-PEG and DSPE-PEG-FA) with the lipid molar ratio of 40:40:10:5:5 was dissolved in 3 mL of chloroform. UCNP (5 mg), CORM (0.5 mg) and α-TOS (1 mg) were also dissolved in the same chloroform mixture. This mixture was then stirred for 4 h, and the organic solvent was evaporated under reduced pressure with a rotary evaporator at 40 ºC. After removal of the organic solvent, the thin film was obtained at the flask bottom and further dried overnight in a desiccator to ensure complete removal of the organic solvent. The thin film was slowly dissolved with HEPES buffer (pH 7.4, 10 mM) under constant stirring at 40 ºC for 4 h. The resultant mixture was sonicated in an ultrasonic water bath for 15 min and centrifuged at 20000 g to obtain the lipid-encapsulated nanoformulation containing UCNPs, CORM and α-TOS (Scheme 1). The final formulation was obtained by dissolving the pellets in HEPES buffer to obtain 1 mg/mL of LUCTF formulation. For LUCF (Lipid/UCNP/CORM/FA) and LUTF (Lipid/UCNP/α-TOS/FA) nanoparticles with a single drug, the same procedure was repeated while using 1 mg of CORM and α-TOS, respectively. Lipid-encapsulated Liss Rhodamine-B PE (30 µg) with and without FA (LURF and LUR) as well as lipid-encapsulated IR-780 (2% w/w) were

View Article Online
DOI: 10.1039/D1BM00941A

also prepared in a dark room for cell uptake and *in vivo* imaging studies using the same thin film hydration method.

Table 1. Nomenclature of all synthesized formulations

Formulation	Materials	Mass (mg)
LUCTF	Lipid/UCNP/CORM/α-TOS/FA	1.43/5/0.5/1/0.07
LUCF	Lipid/UCNP/CORM/FA	1.43/5//1/0.07
LUTF	Lipid/UCNP/α-TOS/FA	1.43/5/1/0.07
LUF	Lipid/UCNP/FA	1.43/5/0.07
LURF	Lipid/UCNP/Rhodamine-B/FA	1.43/5/0.03/0.07
LUR	Lipid/UCNP/Rhodamine-B	1.5/5/0.03
LUF-IR780	Lipid/UCNP/IR-780/FA	1.43/5/0.13/0.07

2.2 Characterization of nanoformulations

The morphology of UCNP, LUCF and LUCTF (lipid formulations stained with 1% phototungsten acid (PTA)) was examined with a Hitachi HT7700A transmission electron microscope (TEM). Fourier Transform Infrared (FTIR) spectroscopy was employed to record the spectra of nanoparticles at every stage of the preparation. The FTIR spectra of dry-powdered nanoparticles were determined in a Thermo Scientific Nicolet 6700 FTIR spectrophotometer. The particle size distribution, zeta potential and colloidal stability of nanoparticles in DMEM (measured every 2 days for 12 days) were determined via dynamic light scattering (DLS) (Nano-ZS Zetasizer, Malvern Instruments).

View Article Online
DOI: 10.1039/D1BM00941A

The amount of pro-drug CORM encapsulated in various nanoformulations was determined by the Mn element content detected with inductively coupled plasma-optical emission spectroscopy (ICP-OES) analysis. The amount of encapsulated α-TOS was determined by dissolving the formulation in DMSO, followed by ultracentrifugation at 40000 g for 1 h to allow the drug content to be determined directly by UV spectroscopic analysis (λ_{ex} = 283 nm). The drugs (CORM and α-TOS) loading (DL) capacity and the encapsulation efficiency (EE) were calculated accordingly.

The photoluminescence (PL) spectra of various nanoparticles (5 mg/mL) were determined in a quartz cuvette by a spectrometer with the excitation wavelength of 980 and 808 nm at 1 W/cm^2. UCNP nanoparticles were dispersed in cyclohexane for PL measurement, while PL spectra of nanoformulations were measured in HEPES buffer.

2.3 *In vitro* CO release triggered by NIR irradiation

The *in vitro* CO release from LUCTF nanoformulation was determined with a synthesized CO fluorescence probe (COFP) described in Dhara et al. [40]. LUCTF formulation in HEPES buffer containing 15 μmol of CORM was added to the CO fluorescent probe (10 μmol) in DMSO. The quartz cuvette containing the mixture was sealed with parafilm throughout the experiment duration to prevent premature CO escape. After irradiation with 808 nm laser (1 W/cm^2 for 5 min), the fluorescence intensity of COFP (λ_{em} = 520 nm) at specific pre-determined time intervals was recorded upon excitation (λ_{ex} = 440 nm) with a fluorescence spectrophotometer (Shimadzu RF 5301-PC).

CO release was also confirmed with FTIR analysis by the intensity change of the characteristic CO vibrations at 2023 and 1928 cm^{-1}. The FTIR spectrum of lyophilized LUCTF (1 mg) was recorded and the same amount of LUCTF in HEPES buffer was irradiated with 808 nm laser (1 W/cm^2 for 5 min), which was then degassed under nitrogen

View Article Online
DOI: 10.1039/D1BM00941A

atmosphere for 1 h. The irradiated sample was lyophilized and its FTIR spectrum was recorded again for comparison.

2.4 Cellular uptake of lipid formulations

Human colorectal carcinoma cell lines (HCT116, ATCC® CCL-247™) were grown in 90% DMEM and supplemented with 10% FBS 100 U/mL penicillin, and 100 µg/mL streptomycin. Exponentially grown cultures were maintained in a humidified chamber containing 5% CO_2 at 37 ℃ throughout the cell studies.

Cell uptake of lipid nanoparticles was assessed with confocal laser scanning microscopy (CLSM). The drugs were replaced with Rhodamine B-lissamine (30 µg) to produce LURF (with FA) and LUR (without FA) for this study. The cells were seeded at a density of 1.5×10^5 cell/well in a 12-well plate with a glass slide at the bottom and cultured for 24 h. The cellular uptake of LURF nanoparticles (20 µg/mL) by HCT116 cells was investigated at different time points (2, 4, and 8 h) with Leica SP8 CLSM. The FA-enhanced uptake was also assessed at 8 h with comparing the cell fluorescence intensity of LUR and LURF. After incubation in the dark, the medium was removed and the cells washed thrice with PBS, followed by staining with DAPI for CLSM imaging.

2.5 Cell viability assay

MTT assay was employed to assess the cell viability after incubation with LUTF, LUCF, LUCF + L, LUCTF and LUCTF + L, where L means 808 nm laser irradiation at 1 W/cm^2 for 5 min. Briefly, HCT116 cells (5×10^3 cell/well) were seeded in a 96-well plate in 100 µL of culture medium after incubation for 24 h. The cells were exposed to 100 µL of FBS-free media containing various concentrations of drugs (0-10 µg/mL for CORM and 0-20 µg/mL for α-TOS), and incubated in the dark. After 3 h, the media in all groups were replaced with

fresh media, and the cells were treated with NIR light (808 nm, 1 W/cm^2) for 5 min. The cells were further incubated for a total of 48 h, followed by 10 µL MTT solution (5 mg/mL) to each well. The medium was removed after 4 h and the contents in each well were dissolved in 100 µL of DMSO. The absorbance was measured with Tecan Infinite M200 PRO Multimode Microplate Reader (Switzerland) at 570 nm using 670 nm as reference wavelength. The cell viability was expressed as a percentage of the untreated cells (control group), as reported elsewhere [41].

2.6 Intracellular CO and ROS detection.

CO release within HCT 116 cells was assessed by incubating treated cells with CO fluorescent probe (10 µmol). Cells (2×10^4) were seeded in 12-well plates with glass slides at the bottom for 24 h. The media were replaced with that containing nanoparticles (15 µmol of CORM) and the cells incubated for 3 h. Then media containing nanoparticles and CO fluorescent probe (10 µmol) were replaced with fresh media, which was irradiated with 808 nm laser at 1 W/cm^2 for 5 min. Cells were continuously incubated for 2 h, washed and fixed with 4 % paraformaldehyde for 15 min, followed by fluorescence imaging (λ_{ex} = 490 nm, λ_{em} = 520 nm).

The ROS generation in cells upon CO release was determined by both qualitative and quantitative methods using 2',7'-dichlorodihydrofluorescein diacetate (DCFH-DA) (10 µmol) probe. For quantitative ROS determination, the cells were analyzed by flow cytometry (Beckman Coulter FC 500) to detect the DCF fluorescence (λex = 488 nm) after treatment. HCT-116 cells in DMEM were seeded in a 48-well plate at a density of 1×10^5 cells/well. After incubation at 37 ºC for 24 h, cell culture media were replaced with that containing nanoparticles (10/5 µg/mL of α-TOS/CORM) for 3 h. The media were replaced with fresh ones containing DCFH-DA and the cells were irradiated with 808 nm laser at 1 W/ cm^2 for 5

View Article Online
DOI: 10.1039/D1BM00941A

min. The treated cells were subsequently collected, washed thrice and harvested in 150 µL of FACS buffer for flow cytometry after DCFH-DA staining for 30 min. For qualitative analysis, the same procedure was followed with cells seeded in wells containing glass slides. After the incubation, DCFH-DA staining and washing procedures, the cells were fixed with 4% paraformaldehyde for 15 min before cell imaging (λ_{ex} = 488 nm, λ_{em} = 530 nm) using a fluorescent microscope (Olympus BX41 light microscope).

2.7 Cell apoptosis assay

Annexin V-FITC assay was employed to determine the cell apoptosis of HCT116 cells (1 × 10^5 cell/well) in 24 well plates. After 24 h, the seeded cells were cultured in media containing nanoparticles (IC_{50} (LUCTF + L) = 2/1 µg/mL of α-TOS/CORM). After 3 h of incubation, media were replaced with fresh ones, followed by irradiation with 808 nm laser at 1 W/ cm^2 for 5 min and further incubated for a total of 24 h. For flow cytometry analysis, all attached and floating cells were collected and washed three times with PBS. The cells were suspended in binding buffer (100 µL), stained with Annexin V-FITC (5 µg/mL) and propidium iodide (PI) (5 µg/mL) for 20 min in the dark. The stained cells were centrifuged andfinally collected in 200500 µL of binding buffer before analysis by flow cytometry.

2.8 JC-1 mitochondria assay

The mitochondrial dye JC-1 (Invitrogen by Thermofischer) was used to determine the mitochondrial membrane potential ($\Delta\Psi_m$) of HCT116 cells after nanoparticle treatment. HCT116 cells were seeded in 24-well plates (2 × 10^5 cell/well) and cultured for 24 h. The cells were then incubated with media containing nanoparticles (10/5 µg/mL of α-TOS/CORM). After incubation for 3 h, media in all groups were replaced and cells were irradiated (808 nm, 1 W/cm^2) for 5 min. Cells were incubated for a total of 8 h, washed and harvested. JC-1 solution (5 µM) was added and incubated with cells for 30 min, followed by

washing with excess buffer, centrifugation at 300 g for 4 min and resuspension in 200 μL of buffer for flow cytometry (λ_{ex} = 488 nm, λ_{em} = 537 nm; λ_{ex} = 535 nm, λ_{em} = 590 nm). Carbonyl cyanide m-chlorophenylhydrazone-CCCP (a mitochondrial electron transport chain inhibitor) at a concentration of 1 μM was incubated with cells for 5 min, which was adopted as a positive control to confirm intensity changes. $\Delta\Psi_m$ was calculated as the ratio between fluorescence intensity at 590 nm and 537 nm, and the percentage of the mean fluorescence intensity of each emission was determined.

2.9 *In vivo* combined cancer therapy

All animal procedures were performed in accordance with the Guidelines for Care and Use of Laboratory Animals of The University of Queensland and approved by the Animal Ethics Committee of The University of Queensland's Office of Research Ethics (# AIBN/224/18), Queensland, Australia. Female BALB/c nude mice (6-8 weeks old) were housed, and allowed to access food and water freely throughout the experiment. The tumor model was established by subcutaneously injecting HCT116 cells (2×10^6) in 100 μl FBS-free medium on the mouse right flank. The tumor size and weight were monitored every other day, and the tumor volume (V) was calculated by the formula: $V = L \times W^2/2$, where L and W represent the longest and the shortest dimension.

The biodistribution of the typical nanoformulation (LUF-IR780) was evaluated by real-time *in vivo* imaging using an NIR fluorescence imaging system (IVIS Lumina X5). Three HCT116 tumor-bearing nude mice with the tumor size of □100 mm^3 were employed for whole-body imaging at 1, 4, 8, 12, and 24 h post tail vein intravenous (iv) injection with LUF-IR780 (10 mg/kg). To further evaluate the targeting ability, the fluorescence intensity of tumors and main organs (heart, liver, spleen, lung, and kidneys) was detected at 12 h and 24 h post iv injection using the ROI function of IVIS Lumina X5 Living Image Software.

View Article Online
DOI: 10.1039/D1BM00941A

Balb/c nude mice were randomly divided into four groups (n = 5) when the tumor volume reached 50-100 mm^3. The mice were treated with PBS, LUCTF, LUCF + L, LUCTF + L, by tail vein iv injection of nanoformulations containing 10 mg/kg of TOS and/or 5 mg/kg of CORM. The drug administration took place on day 0, 3, 6, and 9 with irradiation at 12 h post-treatment (808 nm, 1 W/cm^2 for 5 min). The therapeutic efficacy was assessed by monitoring the tumor volume, and body weight periodically. Two days after the final administration, the mice in each group were sacrificed, and the tumors were weighed and harvested for TUNEL staining. Major organs were also excised for H&E staining to evaluate the safety of the nanoparticles in animals. The tissues were visualized with Olympio BX61 microscope.

2.10 Statistical analysis

The data are presented as mean ± standard error of the mean (SEM) from at least triplicate experiments performed in a parallel manner unless otherwise stated. The differences among the groups were analyzed using one-way analysis of variance (ANOVA), and the significance was indicated as *: $p < 0.05$, **: $p < 0.01$, and ***: $p < 0.001$.

3 Results and Discussion

3.1 Characteristics of lipid-coated CORM-loaded UCNP nanoformulation

Hexagonal oleic acid-capped core-shell UCNPs were synthesized with an average size of 55.6 ± 4.9 nm (**Figure 1A**), as previously reported [42]. The $NaYF_4$: Yb, Tm cores doped with 4.4 nm $NaYF_4$: Nd shell (**Figure S1)** fluoresced upon excitation by both 980 and 808 nm lights. These core-shell UCNPs were used to produce the current nanoformulations, e.g. LUCTF by simultaneous combination of CORM (0.5 mg), α-TOS (1 mg) and lipid mixture

containing DOPC:DOPA:Cholesterol:DSPE-PEG:DSPE-PEG-FA with an optimal molar ratio of 40:40:10:5:5.

Table 2 summarizes the particle size, zeta potential and polydispersity index (PDI) of various nanoparticles with or without drugs (CORM and α-TOS). The hydrodynamic diameters of all nanoparticles were in the range of 130-150 nm, indicating their suitability for cellular uptake and cellular apoptosis studies. LUCTF loaded with both CORM and α-TOS showed a slightly larger particle size (149 ± 2 nm) than that without drugs (LUF, 130 ± 2 nm). Most importantly, the zeta potential of LUTF was slightly negative (-5.9 ± 0.2 mV) upon the addition of α-TOS while the more positively charged CORM partly offsets the negative charges in LUCTF (-3.9 ± 0.2 mV). The zeta potential of LUCF (-1.0 ± 0.2 mV) is close to neutral due to the highly positively charged CORM. The surface charge and size of LUCTF and LUTF were minimally changed after incubation in DMEM mimicking biological fluids at 4 ºC for 12 days (**Figure S2**), indicating the high colloidal stability of these nanoformulations.

As shown in **Figure 1A**, the TEM images show a characteristic lipid appearance surrounding LUCF and LUCTF nanoparticles stained with 1% phosphotungstic acid (PTA) as compared to UCNPs, suggesting that UCNPs were successfully encapsulated into the lipid nanosystem. In order to further confirm the formation of LUCTF, FTIR analysis was employed to assess the qualitative nature of the materials involved in the formulation process (**Figure 1B**). Oleic capped-UCNPs showed characteristic vibrations at 2925, 2852 cm^{-1}, and 1460 cm^{-1}, assigned to CH_3 and CH_2 stretching and C-H bending vibrations, respectively. These characteristic peaks were maintained throughout the formulation procedure as seen in the FTIR spectrum for LUCTF due to the lipid hydrocarbon chains. For CORM, the two characteristic vibrations that represent the CO group were seen at 2023 and 1928 cm^{-1}, and maintained with a slightly lower transmittance in LUCF and LUCTF nanoformulations. The

most prominent vibration confirming the incorporation of α-TOS was observed at 1680 cm^{-1} representing the acyl group (R_2-C=O) in its structure.

Figures 1C and 1D show the photoluminescence (PL) spectra of core-shell UCNPs, LUTF, LUCF and LUCTF in cyclohexane and HEPES buffer, respectively. The lipid encapsulation offered the final UCNP a high hydrophilicity, meanwhile it reduced the PL intensity slightly. Emission of LUCF and LUCTF at around 360 nm was significantly decreased, while that at 450 nm maintained unchanged, which is attributed to specific photon absorbance by encapsulated CORM. Since the amount of CORM was higher in LUCF (10.2 wt%) than in LUCTF (4.63 wt%) (co-encapsulated with 9.2 wt% of α-TOS), LUCF's PL signal at 360 nm was relatively lower than that of LUCTF (**Figure S3**). This phenomenon explains how the UV emission of UCNPs can be absorbed immediately by CORM to trigger CO release for therapeutic purposes.

A major balance between the drug loading and the therapeutic activity was achieved by optimizing the amount of CORM and α-TOS in nanoformulations, as determined by ICP-OES and UV, respectively (**Figure S4)**. **Table S1** shows that the drug loading, the encapsulation efficiency and the yield of LUFT nanoformulation for the highly hydrophobic α-TOS were all enhanced by adding more soluble PEGylated α-TOS (TPGS) in the 1:1 mass ratio of TOS:TPGS. In this case, the LUTF yield was 69.6%, with the drug loading and encapsulation efficiency of 9.98 wt% and 74.9%, respectively. As shown in **Table 2**, CORM had similar drug loading characteristics in LUCF and LUCTF with the drug encapsulation efficiency in both nanoformulations being around 75%. The mass ratio of CORM and α-TOS was maintained at approximately 1:2 in LUCTF, with their loading amounts being 4.63 wt% and 9.20 wt% in the presence of UCNPs, respectively.

View Article Online
DOI: 10.1039/D1BM00941A

Table 2. Particle characteristics of UCNP-based nanoformulations

Samples	Hydrodynamic diameter (nm)	Zeta potential (mV)	Polydispersity index (PDI)	Drug loading (DL, wt%)	Loading efficiency (LE) (%)
LUF	130 ± 2	-5.4 ± 0.1	0.21 ± 0.02	-	-
LUTF	134 ± 3	-5.9 ± 0.2	0.24 ± 0.08	9.98 (α-TOS)	74.9 (α-TOS)
LUCF	145 ± 1	-1.0 ± 0.2	0.24 ± 0.11	10.2 (CORM)	76.5 (CORM)
LUCTF	149 ± 2	-3.9 ± 0.2	0.26 ± 0.03	9.20/4.63*	73.6/74.1*
LUR	140 ± 2	-4.1 ± 0.1	0.22 ± 0.06	-	-
LURF	139 ± 2	-4.4 ± 0.1	0.22 ± 0.04	-	-
LUF-IR780	137 ± 1	-4.1 ± 0.1	0.20 ± 0.04	-	-

*Corresponding DL and EE values of α-TOS and CORM in LUCTF, respectively.

View Article Online
DOI: 10.1039/D1BM00941A

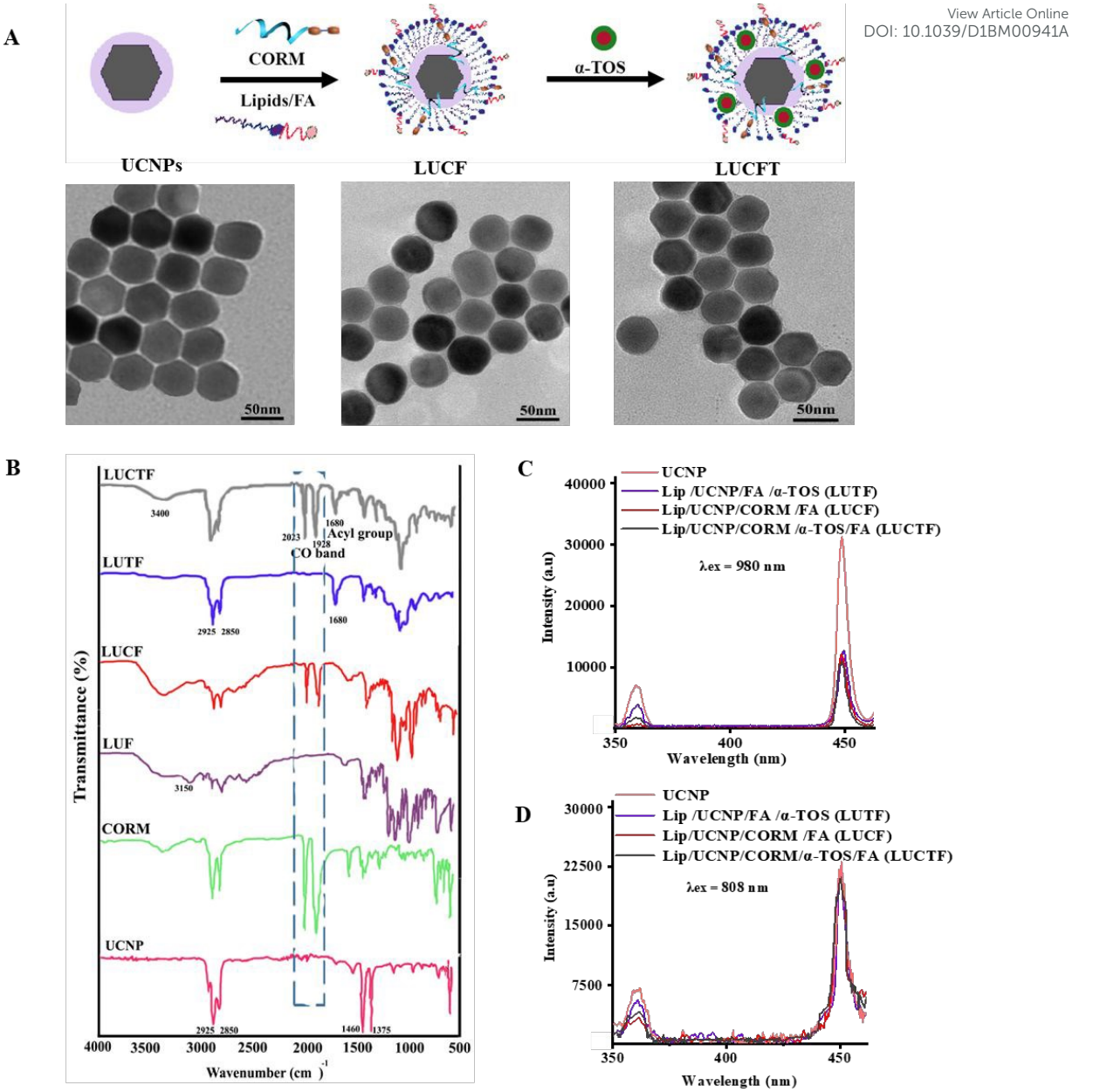

Figure 1. Nanoparticle characteristics. (A) TEM Image of core-shell UCNP, LUCF and LUCTF; **(B)** FTIR Spectra of formulations at different stages from core-shell to α-TOS and CORM modified Lipid-UCNPs (LUCTF). Photoluminescence spectra (1 W/cm^2) of core-shells and formulations at the excitation of; **(C)** 980 nm and **(D)** 808 nm lights.

3.2 NIR-triggered CO release and synergistic cytotoxicity of nanoformulations

NIR-triggered CO release of LUCTF was determined in two ways, i.e. fluorescence spectroscopy using a CO-responsive probe (COFP) [43] and FTIR. As shown in **Figure 2A**, the emission intensity of COFP was maintained minimal without NIR light irradiation. In sharp contrast, COFP's emission was significantly increased upon NIR light irradiation (808 nm, 1 W/cm^2) for 5 min, indicating that CO gas was successfully released from CORMs loaded in LUCTF. The CO release was then confirmed by FTIR analysis (**Figure 2B**). The characteristic CO peaks (2023 and 1928 cm^{-1}) in the spectrum with light irradiation was significantly decreased (about 90%) compared with the original spectrum (before NIR light irradiation), indicating that most CO molecules were released from CORMs after 808 nm laser irradiation.

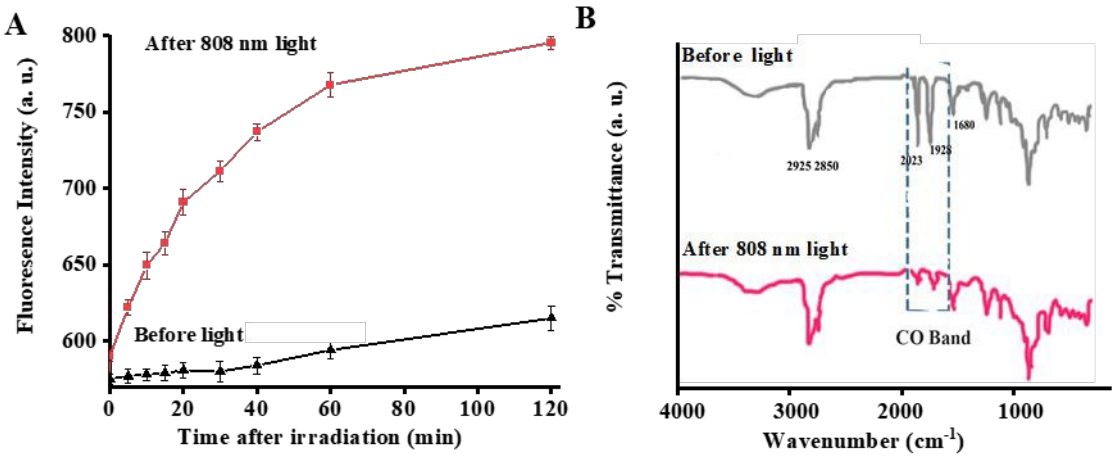

Figure 2. CO release from CORM in LUCTF. (A) CO release profile from LUCTF in the presence of CO fluorescent probe (λ_{ex}= 440 nm and λ_{em} = 520 nm) in HEPES buffer before and after light irradiation for 5 min at 1 W/cm^2**; (B)** FTIR spectra of LUCTF before and after 808 nm light irradiation for 5 min at 1 W/cm^2.

Figure 3A and **3B** show that the cellular uptake of the nanoformulations was very rapid and appeared to peak at 8 h. During incubation around 4-8 h, about 15% increase in

View Article Online
DOI: 10.1039/D1BM00941A

mean fluorescence intensity (MFI) was observed. Moreover, the incorporation of folates enhanced the cellular uptake, as evidenced by the significant difference in the mean fluorescence intensity of HCT116 cells incubated with LURF and LUR for 8 h (**Figure 3B**). In fact, the fluorescence intensity of cells incubated with LUR for 8 h was only close to that of cells incubated for 2 h with FA-tagged LURF. These data indicate that FA significantly contributed to targeting HCT116 cancer cells with overexpressed folic acid (FA) receptors.

As shown in **Figure S5A**, drug-free lipid nanoformulation (LUF) showed negligible toxicity to HCT116 cells even at the concentration up to 200 μg/mL with or without 808 nm irradiation (1 W/cm^2, 5 min). This suggests that carrier materials were biocompatible, without any detectable cytotoxicity. Nanoformulations LUTF and LUCF showed a dose-dependent cytotoxicity, with the IC_{50} value of 10.6 (α-TOS) and 43.9 (CORM), respectively, without NIR irradiation (**Figure S5B, Table S3**). Upon 808 nm laser irradiation for 5 min at 1 W/cm^2, the viability profile of cells treated with LUTF was similar to that without NIR irradiation, while the viability of cells treated with LUCF and laser was significantly reduced, with the CORM IC_{50} value reduced significantly to 5.11 μg/mL (**Figure 3C, Table S3**). The significant reduction of IC_{50} is attributed to the CO release initiated by the conversion of 808 nm lights to 360 nm photons as mediated by UCNPs in LUCF. Based on the IC_{50} values of LUTF (α-TOS) and LUCF (CORM) with the laser irradiation, the combination with the α-TOS: CORM mass ratio of 2:1 in one nanoparticle may be optimal, i.e. formulated in the current LUCTF nanoformulation (**Table 2**).

As shown in **Figure S5**, LUCTF nanoparticles with two drugs led to lower cell viability, even without NIR irradiation. Their combination effect could be simply additive as the combination index was 1.04. Together with NIR irradiation, the combination of two drugs in LUCTF nanoparticles induced much more cells to apoptosize, with the average combination index (CI) of 1.26 in **Table S2**, indicating a moderately synergistic effect [44, 45].

View Article Online
DOI: 10.1039/D1BM00941A

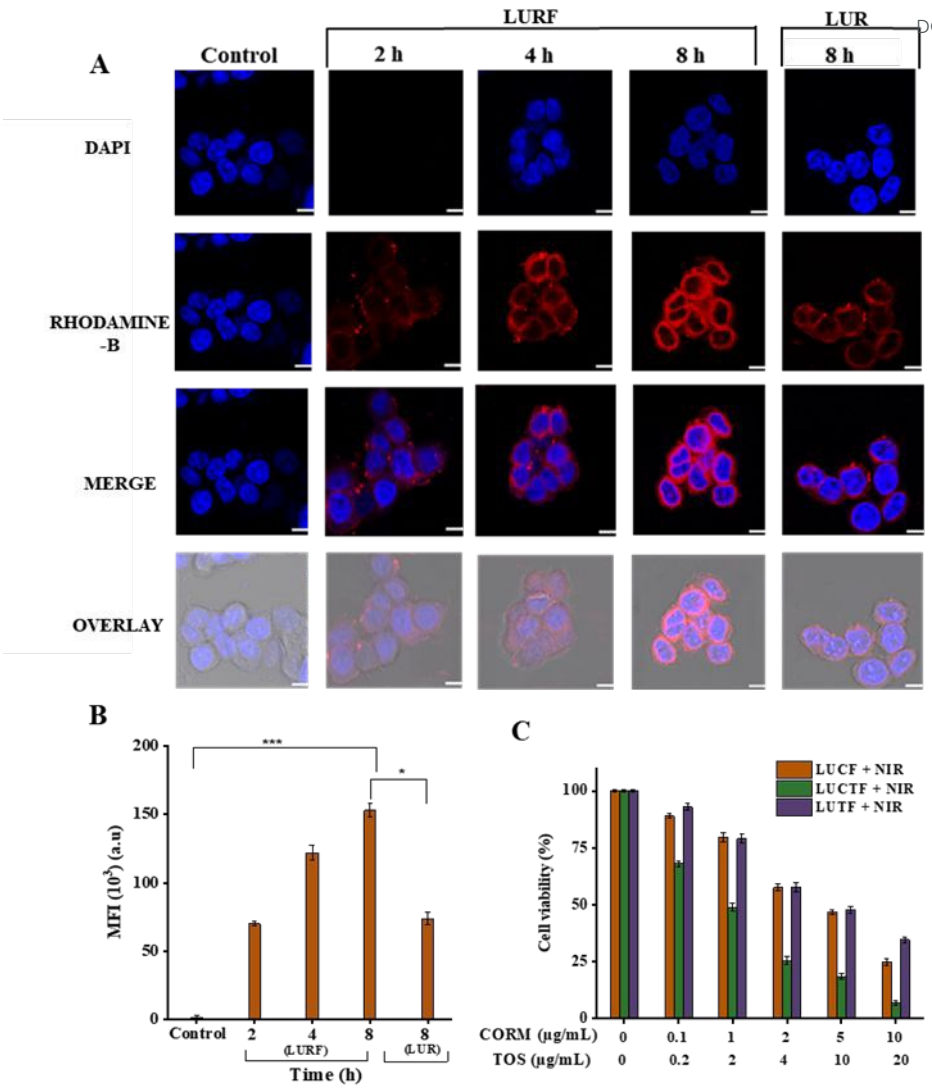

Figure 3. ***In vitro*** **cellular uptake and cytotoxicity of LUCTF. (A)** Fluorescence imaging where Rhodamine-B was loaded into lipid layer and used to label LURF and LUR nanoparticles; **(B)** mean fluorescence intensities after incubation of HCT 116 cells with FA (LURF) and without FA (LUR) for different times; and **(C)** MTT assay of HCT 116 cells incubated with LUCF, LUTF, and LUCTF for 3 h before replacing cell media and then irradiation (808 nm, 1 W/cm^2) for 5 min, followed by 44 h continuous incubation.

3.3 Mechanisms for *in vitro* chemophototherapy

View Article Online
DOI: 10.1039/D1BM00941A

DCFH-DA probe was employed to ascertain the level of intracellular ROS with respect to the therapeutic action of CO and α-TOS. As shown in **Figure 4A** and **4C**, the generation of ROS in LUTF/LUCTF-treated cells was clearly observed without NIR irradiation, suggesting that α-TOS contributed to moderate ROS generation in cancer cells. Upon NIR light irradiation, ROS production in LUCF and LUCTF incubated cells was significantly increased, with the latter cells producing the highest ROS level among all groups. The fluorescence images were well corresponding to the ROS flow cytometry analysis (**Figure S6**). The ROS fluorescence intensity is well correlated with the cell viability (**Figure S7A**), suggesting that the ROS generation was primarily driven by CO release in the presence of α-TOS, and has a greater contribution to the apoptotic therapy [46].

Figure 4B and 4D further present the fluorescence signal of CO release in HCT 116 cells. Upon NIR light irradiation, the intracellular fluorescence intensity of COFP probes was significantly higher (3.7 times) than that of the group without irradiation. This means that released CO molecules in cells provide the necessary therapeutic action via the direct correlation between the CO amount and the characteristic ROS generation level (**Figure S7B)**. Note that the weaker COFP fluorescence intensity of HCT 116 cells incubated with LUCTF without NIR irradiation may be attributed to the limited fenton-like reaction in intracellular H_2O_2 [47, 48]and the casual room light.

PI-Annexin V FITC was employed to quantify the apoptotic and necrotic cell populations under different treatment conditions. As demonstrated in **Figure 4E** and **S8**, the number of apoptotic cells was negligible (94.7% viable) in the control group. The quantitative data confirmed 70.3% and 54.6% viable cells for the LUCTF-treated group before and after NIR light irradiation, respectively. The synergistic group (LUCTF + L) resulted in about 31.2% late apoptotic cells and 5.24% early apoptotic cells. Similarly, the LUCF group produced a very low apoptotic effect (88.2 % viable cells), but the effect was

View Article Online
DOI: 10.1039/D1BM00941A

markedly increased under light irradiation (71.8 % viable cells). The apoptotic effect produced by the various groups well correlates with the cell viability assay (**Figure 3C**), suggesting that the combined effect of both therapeutic agents after irradiation could significantly induce the cell apoptosis at its IC_{50} value.

The mitochondrial membrane potential (MMP or $\Delta\Psi_m$) was also assessed with JC-1 assay to determine the state of the mitochondria after different treatments. This potential differentiates between energized and de-energized mitochondria when the normal green fluorescent dye molecules form aggregates with red fluorescence after targeting energized mitochondria in response to the higher membrane potential [49]. **Figure 4F** shows that the green fluorescence (J-monomer) was increased more or less among the groups treated with various nanoformulations in comparison with the control group, suggesting a lower MMP (loss of mitochondria integrity) after the treatments. The LUTF incubation produced red and green fluorescence with a $\Delta\Psi_m$ ratio of 49:51, indicating that the LUTF nanoparticles could instigate mitochondrial collapse. Relatively, the LUCF group presented a very low green fluorescence without NIR light irradiation ($\Delta\Psi_m$ ratio of 76:24), but a relatively stronger green fluorescence ($\Delta\Psi_m$ ratio of 57:43) was observed after NIR light irradiation. LUCTF group produced a red to green fluorescence ratio of about 44:56 and 31:69 before and after NIR light irradiation, suggesting that the combination of therapeutic agents significantly increased the action on the mitochondria to trigger its collapse. It is clear that the actions of both CO and α-TOS are related to the characteristic changes in the mitochondria. This is because CO is known to alter the mitochondrial respiratory chain at the cytochrome *c* oxidase level, and α-TOS targets the mitochondrial complex II to render the mitochondrial outer membrane permeable [50].

View Article Online
DOI: 10.1039/D1BM00941A

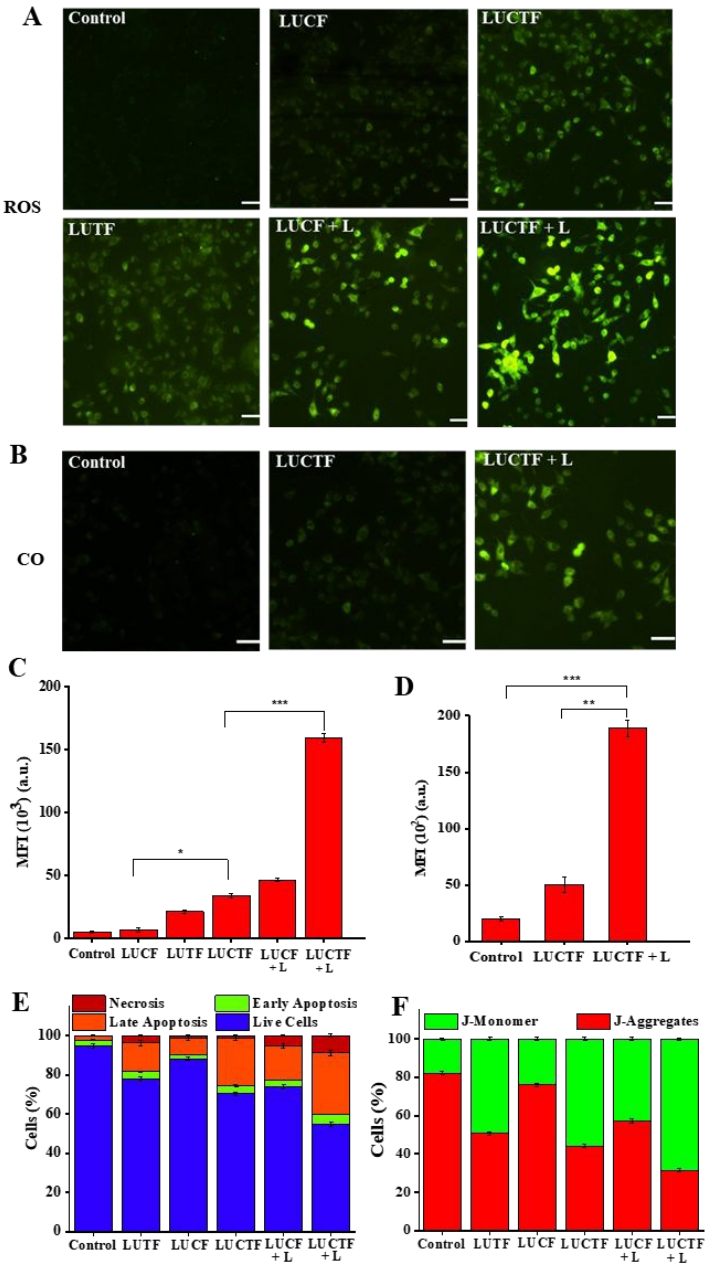

Figure 4. Mechanism for *in vitro* actions of nanoformulations. (A) Fluorescent images after 30 min staining with DCFH-DA (λ_{ex} = 490 nm, λ_{em} = 525 nm) indicating ROS generation in HCT 116 cells treated with LUCTF, LUCF, LUTF (10 µg/mL - drug concentration) for 3 h before nanoparticle removal, irradiation and staining ; **(B)** Intracellular CO release images (λ_{ex} = 440 nm, λ_{em} = 520 nm) of HCT 116 cells treated with LUCTF (15 µM of CORM) for 3 h, followed by staining and 2 h incubation; **(C)** MFI of flow cytometry analysis for ROS detection; (**D**) MFI of flow cytometry analysis for CO release detection; **(E)**

Cellular apoptosis of HCT116 cells incubated for 3 h followed by various treatments similar to (A) before staining at 24 h; **(F)** Flow cytometry analysis for JC-1 mitochondria integrity of HCT116 incubated with nanoparticles for 3 h, followed by various treatments and 5 h incubation. In each *in vitro* test, various treatments included replacement of media with nanoparticles with fresh media at 3 h, followed by NIR irradiation (808 nm, 1 W/cm^2, 5 min) and cell staining, if designed.

3.4 Efficient *in vivo* combination therapy

Firstly, the systemic biodistribution of IR-780-loaded nanoparticles (LUF-IR780) was assessed by real time *in vivo* imaging after tail vein administration. As shown in **Figure 5A**, after 1 h of injection, the nanoparticles clearly accumulated at the tumor site as well as in the lung. The accumulation in tumor tissues was significantly increased from 4 to 24 h. The accumulation in the lung was relatively quicker, as lipid nanoparticles in the absence of targeting agents are known to preferentially accumulate in the lung [51-54]. The nanoparticles were not significantly directed into other organs, such as spleen, kidney and heart, but a low amount was detected in the liver (**Figure 5B, S9**). This suggests that the nanoparticles could be directed to the tumor site, even with a relatively small tumor with the size around 50-100 mm^3, probably due to the enhanced permeation and retention (EPR) effect and FA targeting to the folate receptors over-expressed on HCT-116 tumor cells.

The therapeutic efficacy of the combination of CORM and α-TOS in these lipid-based nanoformulations was then assessed by a scheduled intravenous (iv) administration to HCT116 tumor-bearing nude mice. As shown in **Figure 6A** and 6**C**, LUCF + L and LUCTF showed a moderate degree of tumor inhibition as compared to the control group, by 53.4% ± 1.6% and 35.9% ± 1.8%, respectively, at day 12. Remarkably, LUCTF + L proved to be much more efficient in terms of the sustained reduction of tumor growth, by 87.4% ± 1.8% at

View Article Online
DOI: 10.1039/D1BM00941A

day 12 after 4 administrations (**Figure 6C**). The tumor size measured in the LUCTF + L group was not increased, which means that the tumor growth was successfully inhibited until the end of the study. This tumor size is consistent with the tumor weight at day 12, being 88.1% ± 1.8%, 52.3% ± 1.7% and 37.1% ± 1.8% less, respectively for LUCTF + L, LUCF + L and LUCTF groups, in comparison with the control group (**Figure 6D**). . The high combination efficacy of α-TOS and CORM under irradiation in the tumor growth inhibition can be attributed to their mild synergy at the carefully selected mass ratio, due to the locally triggered CO generation to change the mitochondrial respiratory chain at the cytochrome c oxidase level and α-TOS caused permeation of the mitochondrial outer membrane *via* the mitochondrial complex II, which orchestrates to induce cancer cell death [11, 55, 56].

As shown in **Figure 6B**, the cells stained with TUNEL in the control group produced a pale blue fluorescence, but this fluorescence was completely absent in the LUCTF + L group due to the apoptotic nature of these treated cancer cells. LUCTF group also produced a limited percentage of apoptotic cells, which was slightly lower than that in the LUCF + L group, indicating that the released CO was slightly more effective than that of α-TOS in LUCTF.

There was no observed significant loss of the whole body weight in all groups throughout the study (**Figure 6E**). The increase in the tumor size of the control group resulted in a net weight gain. Furthermore, **Figure 5C** demonstrates that there were no obvious changes in the tissue histopathology of major organs compared to the control group, demonstrating a good biosafety and biocompatibility of the nanoformulations within the period of drug administration.

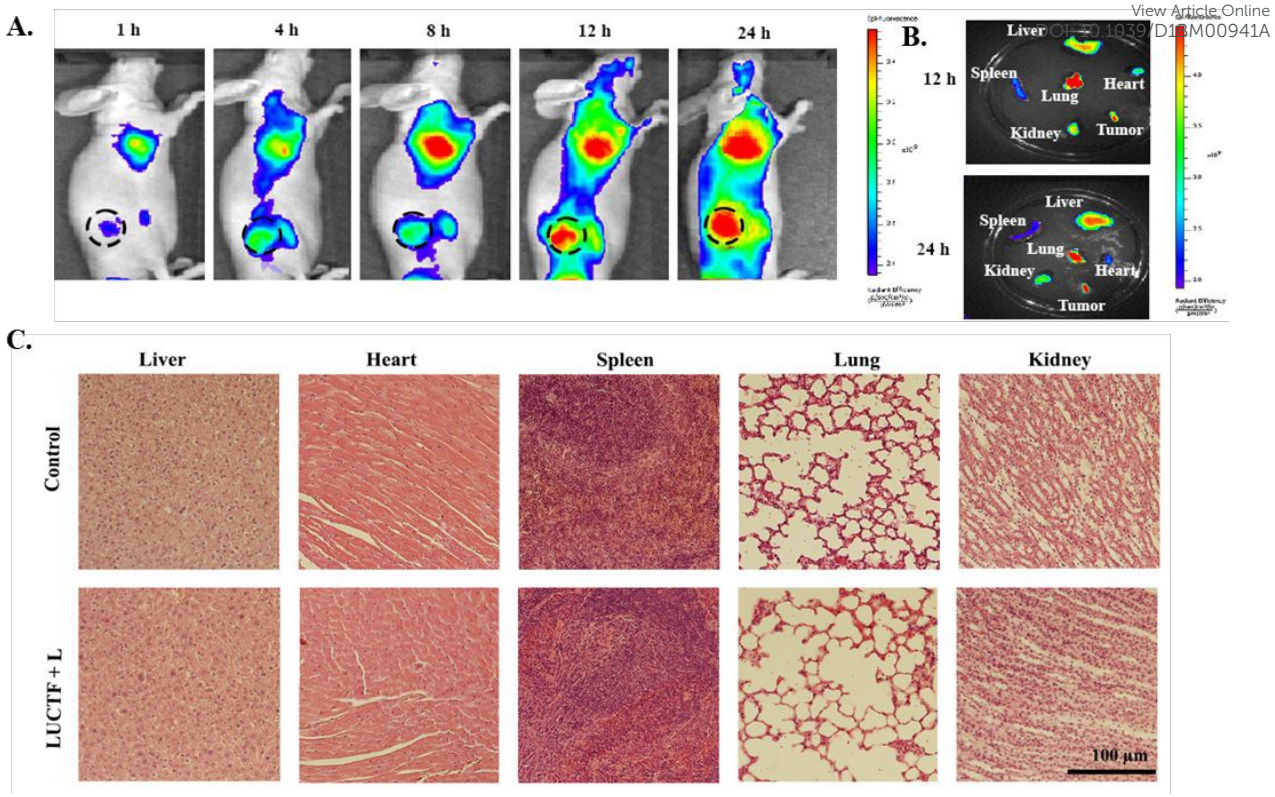

Figure 5. Biodistribution and safety of LUCTF. (A) *In vivo* imaging of HCT116 tumor-bearing nude mice administered with LUF-IR780 at various time points**; (B)** Representative *ex vivo* images of major organs collected at 12 h and 24 h post-injection; and **(C)** Histological images of tissues stained with H & E indicating the status of major organs after animals were sacrificed at day 12 post iv injection.

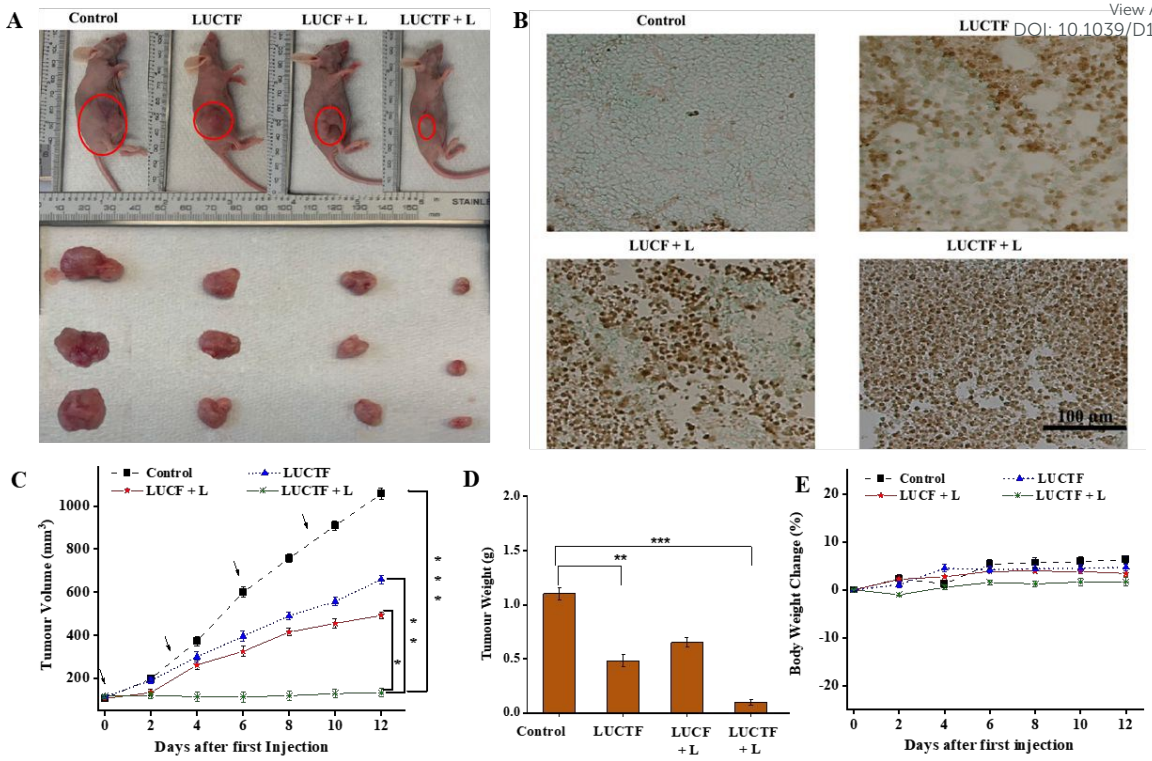

Figure 6. ***In vivo*** **therapeutic effect. (A)** Images of mice bearing tumors and tumors harvested at 12 days of nanoformulation administration; **(B)** Histological images of tumor tissues stained with TUNEL; **(C)** Tumor volume changes during the treatment; **(D)** Tumor weight after 12 days; and **(E)** The average body weight of mice during the treatement. iv injection at Day 0, 3, 6 and 9 at 10 mg/kg of α-TOS and 5 mg/kg of CORMs, and NIR irradiation at 12 h after each injection (808 nm, 1 W/cm^2 for 5 min) if designed.

4 Conclusion and Future Prospect

In this work, we first demonstrated that UCNPs converted NIR lights to produce high energy UV photons (360 nm) to trigger the cleavage and release of CO molecules. The lipid-coated nanoformulation was capable of co-encapsulating a CO-containing metal complex (CORM) and Vitamin E analogue in the mixed form of pegylated and non-pegylated α-TOS. The combined roles of α-TOS and CORM under irradiation in a carefully selected ratio were better positioned to inhibit cancer cell growth as it produced a mildly synergistic effect as

compared to the other nanoformulations. We further demonstrated that the FA-conjugated LUCTF nanoparticle preferentially accumulated in tumor tissues and efficiently prevented tumor progression with a good safety profile in major organs. This nanoformulation could be further developed as a promising nanodrug for targeted cancer gas therapy using the lipid delivery systems combined with suitable amounts of α-TOS.

Conflict of interest

The authors declare that there are no competing interests regarding this paper.

Acknowledgements

The authors acknowledge financial supports from Australian Research Council (ARC) Discovery Projects (DP190103486). Y. O-D. gratefully acknowledges the Australian Government Research Training Program Scholarship (RTP). The authors also give thanks to facilities and the technical assistance of the Australian Microscopy & Microanalysis Research Facility at the Centre for Microscopy and Microanalysis (CMM), Australian National Fabrication Facility (QLD Node) and Centre of Advance Imaging, The University of Queensland.

References

1. I. Bozic, J. G. Reiter, B. Allen, T. Antal, K. Chatterjee, P. Shah, Y. S. Moon, A. Yaqubie, N. Kelly, D. T. Le, E. J. Lipson, P. B. Chapman, L. A. Diaz, Jr., B. Vogelstein and M. A. Nowak, *Elife*, 2013, **2**, e00747.
2. J. S. Lopez and U. Banerji, *Nature Reviews Clinical Oncology*, 2017, **14**, 57-66.
3. R. S. Narayan, P. Molenaar, J. Teng, F. M. G. Cornelissen, I. Roelofs, R. Menezes, R. Dik, T. Lagerweij, Y. Broersma, N. Petersen, J. A. Marin Soto, E. Brands, P. van Kuiken, M. C. Lecca, K. J. Lenos, S. G. J. G. In 't Veld, W. van Wieringen, F. F. Lang, E. Sulman, R. Verhaak, B. G. Baumert, L. J. A. Stalpers, L. Vermeulen, C.

Watts, D. Bailey, B. J. Slotman, R. Versteeg, D. Noske, P. Sminia, B. A. Tannous, T. Wurdinger, J. Koster and B. A. Westerman, *Nature Communications*, 2020, **11**, 2935.

4. J. H. Doroshow and R. M. Simon, *Cell*, 2017, **171**, 1476-1478.
5. R. J. Tallarida, *Genes Cancer*, 2011, **2**, 1003-1008.
6. Y. Opoku-Damoah, A. G. Assanhou, M. A. Sooro, C. A. Baduweh, C. Sun and Y. Ding, *ACS Appl Mater Interfaces*, 2018, **10**, 14231-14247.
7. C. Szabo, *Nat Rev Drug Discov*, 2016, **15**, 185-203.
8. A. Nakao, R. Sugimoto, T. R. Billiar and K. R. McCurry, *Journal of clinical biochemistry and nutrition*, 2009, **44**, 1-13.
9. M. J. Alcaraz, M. I. Guillen, M. L. Ferrandiz, J. Megias and R. Motterlini, *Curr Pharm Des*, 2008, **14**, 465-472.
10. R. Motterlini, B. E. Mann, T. R. Johnson, J. E. Clark, R. Foresti and C. J. Green, *Curr Pharm Des*, 2003, **9**, 2525-2539.
11. B. Wegiel, D. Gallo, E. Csizmadia, C. Harris, J. Belcher, G. M. Vercellotti, N. Penacho, P. Seth, V. Sukhatme, A. Ahmed, P. P. Pandolfi, L. Helczynski, A. Bjartell, J. L. Persson and L. E. Otterbein, *Cancer research*, 2013, **73**, 7009-7021.
12. W. Halina, D. Jozef and J. Alicja, *Current Drug Targets*, 2010, **11**, 1551-1570.
13. L. E. Otterbein, F. H. Bach, J. Alam, M. Soares, H. Tao Lu, M. Wysk, R. J. Davis, R. A. Flavell and A. M. K. Choi, *Nature Medicine*, 2000, **6**, 422.
14. Z. Jin, Y. Wen, L. Xiong, T. Yang, P. Zhao, L. Tan, T. Wang, Z. Qian, B.-L. Su and Q. He, *Chemical Communications*, 2017, **53**, 5557-5560.
15. Q. He, D. O. Kiesewetter, Y. Qu, X. Fu, J. Fan, P. Huang, Y. Liu, G. Zhu, Y. Liu, Z. Qian and X. Chen, *Advanced Materials*, 2015, **27**, 6741-6746.
16. A. E. Pierri, P.-J. Huang, J. V. Garcia, J. G. Stanfill, M. Chui, G. Wu, N. Zheng and P. C. Ford, *Chemical Communications*, 2015, **51**, 2072-2075.
17. J. Yao, Y. Liu, J. Wang, Q. Jiang, D. She, H. Guo, N. Sun, Z. Pang, C. Deng, W. Yang and S. Shen, *Biomaterials*, 2019, **195**, 51-62.
18. Z. Shi, K. Zhang, S. Zada, C. Zhang, X. Meng, Z. Yang and H. Dong, *ACS Applied Materials & Interfaces*, 2020, **12**, 12600-12608.
19. Y. Opoku-Damoah, R. Zhang, H. T. Ta, D. Amilan Jose, R. Sakla and Z. Ping Xu, *Eur J Pharm Biopharm*, 2020, DOI: 10.1016/j.ejpb.2020.11.014.
20. D. Wu, X. Duan, Q. Guan, J. Liu, X. Yang, F. Zhang, P. Huang, J. Shen, X. Shuai and Z. Cao, *Advanced Functional Materials*, 2019, **29**, 1900095.
21. Y. Li, J. Dang, Q. Liang and L. Yin, *Biomaterials*, 2019, **209**, 138-151.

22. L. M. Wiesholler, F. Frenzel, B. Grauel, C. Würth, U. Resch-Genger and T. Hirsch, *Nanoscale*, 2019, **11**, 13440-13449.

23. J. E. Choi, H.-K. Kim, Y. Kim, G. Kim, T. S. Lee, S. Kim, D. Kim and H. S. Jang, *Materials & Design*, 2020, **195**, 108941.

24. X. Zhang, X. Peng, W. Yu, S. Hou, Y. Zhao, Z. Zhang, X. Huang and K. Wu, *Cancer Letters*, 2011, **307**, 174-181.

25. A. Mallick, P. More, S. Ghosh, R. Chippalkatti, B. A. Chopade, M. Lahiri and S. Basu, *ACS Applied Materials & Interfaces*, 2015, **7**, 7584-7598.

26. L. F. Dong, P. Low, J. C. Dyason, X. F. Wang, L. Prochazka, P. K. Witting, R. Freeman, E. Swettenham, K. Valis, J. Liu, R. Zobalova, J. Turanek, D. R. Spitz, F. E. Domann, I. E. Scheffler, S. J. Ralph and J. Neuzil, *Oncogene*, 2008, **27**, 4324-4335.

27. M. Tomasetti, L. Nocchi, J. Neuzil, J. Goodwin, M. Nguyen, L. Dong, N. Manzella, S. Staffolani, C. Milanese, B. Garrone, R. Alleva, B. Borghi, L. Santarelli and R. Guerrieri, *PLOS ONE*, 2012, **7**, e52263.

28. Y.-H. Kang, E. Lee, M.-K. Choi, J.-L. Ku, S. H. Kim, Y.-G. Park and S.-J. Lim, *International Journal of Cancer*, 2004, **112**, 385-392.

29. L. Prochazka, L. F. Dong, K. Valis, R. Freeman, S. J. Ralph, J. Turanek and J. Neuzil, *Apoptosis : an international journal on programmed cell death*, 2010, **15**, 782-794.

30. L. F. Dong, P. Low, J. C. Dyason, X. F. Wang, L. Prochazka, P. K. Witting, R. Freeman, E. Swettenham, K. Valis, J. Liu, R. Zobalova, J. Turanek, D. R. Spitz, F. E. Domann, I. E. Scheffler, S. J. Ralph and J. Neuzil, *Oncogene*, 2008, **27**, 4324-4335.

31. L.-F. Dong, R. Freeman, J. Liu, R. Zobalova, A. Marin-Hernandez, M. Stantic, J. Rohlena, K. Valis, S. Rodriguez-Enriquez, B. Butcher, J. Goodwin, U. T. Brunk, P. K. Witting, R. Moreno-Sanchez, I. E. Scheffler, S. J. Ralph and J. Neuzil, *Journal of Biological Chemistry*, 2009, **15**, 1593-1600.

32. Š. Koudelka, J. Mašek, J. Neuzil and J. Turánek, *Journal of Pharmaceutical Sciences*, 2010, **99**, 2434-2443.

33. C. M. Neophytou and A. I. Constantinou, *BioMed Research International*, 2015, **2015**, 584862.

34. R. S. Fernandes, J. O. Silva, H. A. Seabra, M. S. Oliveira, V. M. Carregal, J. M. C. Vilela, M. S. Andrade, D. M. Townsend, P. M. Colletti, E. A. Leite, V. N. Cardoso, L. A. M. Ferreira, D. Rubello and A. L. B. Barros, *Biomedicine & pharmacotherapy = Biomedecine & pharmacotherapie*, 2018, **103**, 1348-1354.

35. Y. Wu, J. Liu, F. Movahedi, W. Gu, T. Xu and Z. P. Xu, *Advanced Healthcare Materials*, 2020, **9**, 1901706.

36. J.-R. Alonso, F. Cardellach, S. López, J. Casademont and Ò. Miró, *Pharmacol Toxicol*,
2003, **93**, 142-146.

37. L. Dong and J. Neuzil, *Cancer Communications*, 2019, **39**, 63.

38. K. Kluckova, A. Bezawork-Geleta, J. Rohlena, L. Dong and J. Neuzil, *Biochimica et Biophysica Acta (BBA) - Bioenergetics*, 2013, **1827**, 552-564.

39. R. Sakla and D. A. Jose, *ACS Appl Mater Interfaces*, 2018, **10**, 14214-14220.

40. K. Dhara, S. Lohar, A. Patra, P. Roy, S. K. Saha, G. C. Sadhukhan and P. Chattopadhyay, *Anal Chem*, 2018, **90**, 2933-2938.

41. D. Aouameur, H. Cheng, Y. Opoku-Damoah, B. Sun, Q. Dong, Y. Han, J. Zhou and Y. Ding, *Nano Research*, 2018, **11**, 4245-4264.

42. Y. Opoku-Damoah, R. Zhang, H. T. Ta, D. Amilan Jose, R. Sakla and Z. P. Xu, *European Journal of Pharmaceutics and Biopharmaceutics*, 2021, **158**, 211-221.

43. B. Das, S. Lohar, A. Patra, E. Ahmmed, S. K. Mandal, J. N. Bhakta, K. Dhara and P. Chattopadhyay, *New Journal of Chemistry*, 2018, **42**, 13497-13502.

44. B. Li, J. Tang, W. Chen, G. Hao, N. Kurniawan, Z. Gu and Z. P. Xu, *Biomaterials*, 2018, **177**, 40-51.

45. A. Ito, M. Fujioka, T. Yoshida, K. Wakamatsu, S. Ito, T. Yamashita, K. Jimbow and H. Honda, *Cancer Science*, 2007, **98**, 424-430.

46. P. M. Yang, Y. T. Huang, Y. Q. Zhang, C. W. Hsieh and B. S. Wung, *Vascul Pharmacol*, 2016, **87**, 209-218.

47. Y. Wang, Z. Liu, H. Wang, Z. Meng, Y. Wang, W. Miao, X. Li and H. Ren, *Acta Biomaterialia*, 2019, **92**, 241-253.

48. Z. Jin, Y. Wen, L. Xiong, T. Yang, P. Zhao, L. Tan, T. Wang, Z. Qian, B. L. Su and Q. He, *Chem Commun (Camb)*, 2017, **53**, 5557-5560.

49. A. Perelman, C. Wachtel, M. Cohen, S. Haupt, H. Shapiro and A. Tzur, *Cell Death & Disease*, 2012, **3**, e430-e430.

50. J. Kang and S. Pervaiz, *Biochemistry Research International*, 2012, **2012**, 896751.

51. O. B. Garbuzenko, M. Saad, S. Betigeri, M. Zhang, A. A. Vetcher, V. A. Soldatenkov, D. C. Reimer, V. P. Pozharov and T. Minko, *Pharmaceutical Research*, 2008, **26**, 382.

52. K. Pal, V. S. Madamsetty, S. K. Dutta and D. Mukhopadhyay, *Int J Nanomedicine*, 2019, **14**, 5109-5123.

53. X. Qiu, Z. Li, X. Han, L. Zhen, C. Luo, M. Liu, K. Yu and Y. Ren, *Theranostics*, 2019, **9**, 2618-2636.

54. R. Wang, C. Zhang, J. Li, J. Huang, Y. Opoku-Damoah, B. Sun, J. Zhou, L. Di and Y. Ding, *Biomaterials*, 2019, **221**, 119413.

55. T. I. Ayudhya, P. J. Pellechia and N. N. Dingra, *Dalton Transactions*, 2018, **47**, 538-543.

56. D. R. Hess, *Respiratory Care*, 2017, **62**, 1333-1342.